Journal Name

ARTICLE TYPE

Cite this: DOI: 00.0000/xxxxxxxxxx

Strategic Design of Tri-Metallic Structure Electrocatalysts for Prompting Enhanced Charge Transfer Effects in the Electrochemical Reduction of CO_2

Ian Brewis,[a] Sankeerthana Bellamkonda,[a*] Venkateswara Rao Gedela,[a] Rana-Faisal Shahzad,[a] Abdesslem Jedidi,[b] and Shahid Rasul[a*]

Received Date
Accepted Date

DOI: 00.0000/xxxxxxxxxx

The lack of availability of efficient, selective, and stable electrocatalysts is a major hindrance to the scalability of the CO_2 reduction processes. The use of Cu with Indium (In) and Tin (Sn) to form bimetallic composite electrocatalyst materials has been shown, from our pioneering work, to greatly improve selectivity of CO_2 reduction through changes in morphology and electronic structure [1–3]. Such changes were a result of the suppression of the HER, whilst showing only a slight weakening of the adsorption energy of CO. Due to the mild poisoning of active sights through In incorporation however, Cu_2O/In electrodes have previously demonstrated only mild current densities. By incorporating highly conductive Pt within the electrode back contact GDL, we aim to develop upon prior electrocatalyst designs by overcoming this key limitation of electrode activity. Herein, we report a pioneering study into the dynamics of cutting-edge tri-metallic electrocatalysts, providing activity enhanced electrodes through Pt incorporation. Experimental results demonstrate how the incorporation of nano-thickness interfacial Pt layers within the catalyst bulk provides a facile method of activity control within a given range. Using a Pt-enriched GDE layer, current densities up to -204 $mAcm^{-2}$ at -1.5 V vs RHE were observed, demonstrating a 183% improvement in electrocatalyst activity over that of Cu_2O/In. Pt deposition within 2 μm of the electroactive surface additionally demonstrates highly consistent partial current densities for CO_2 reduction products over a 24 hour period, suggesting Pt incorporation to provide minimal reduction in electrode stability with prolonged use. The study herein provides a cutting-edge method of enhancing electrocatalytic performance of previous Cu_2O/In electrocatalyst designs through tailored, sub-surface Pt layer deposition.

1 Introduction

In recent years, the reduction of CO_2 via electrochemical methods, in particular, has begun to see notable interest within the field of electrochemistry due to its ability to reduce CO_2 to fuels and value-added chemicals under ambient conditions [4–8]. The electrochemical reduction of CO_2 however is still an emerging technology which has yet to be implemented regularly on an industrial scale. Significant challenges currently limit electrochemical CO_2 reduction to lab-scale operation including, issues regarding energy efficiency of the electrochemical fuel cells, limited reaction selectivity both between CO_2 reduction (CO_2R) products and with the competing hydrogen evolution reaction (HER), as well as overall CO_2 conversion rates. In most cases, such issues arise as a result of the material properties of the cathodic electrocatalyst material, thus before carbonaceous fuels produced via the reduction of CO_2 can be considered as a viable method of energy storage, each of these challenges must first be addressed [8,9].

A key method in the development of next-generation electrocatalysts is in the incorporation of additional metal centres on Cu-based electrocatalyst surfaces [1,2,10–13]. Each material in turn come with their own merits and sustainable issues. In order to upscale electrochemical CO_2 reduction to be a cost-effective process, the combination of multiple non-noble metal bimetallic electrocatalysts such as Cu/In [1,2,14] and Cu/Sn [3,15,16] have been seen to offer a practical solution in implementing electrocatalysts on an industrial scale. Cu/In and Cu/Sn electrocatalysts in particular have been shown previously to drastically suppress HER in favour of CO. Hang et al. [17] for example, demonstrated a Cu/In electrocatalyst capable of producing greater than 90% Faradaic efficiency (FE) toward CO formation, with only ≈5% of the total FE being leeched by competing HER.

Cu/In-based electrocatalysts however, are often hindered by both their low binding energy of CO and mild activity which often

[a] Faculty of Engineering and Environment, Northumbria University, Ellison Pl, Newcastle Upon Tyne, NE1 8ST, UK. E-mail: Shahid.Rasul@Northumbria.ac.uk; sankeerthana999@gmail.com
[b] Department of Chemistry, King AbdulAziz University, Abdullah Sulayman, Kingdom of Saudi Arabia - Jeddah, 21589, Saudi Arabia

hinders their effectiveness in producing multi-carbon compounds at industry relevant current densities. The key reasoning behind this has been linked to the inclusion of In, whereby In incorporation results in both the slight reduction in the adsorption strength of CO, as well as a reduction in the number of surface active sites, resulting in an overall reduced performance in both the selectivity toward higher-order products, and electrocatalytic activity, respectively [2].

By limiting the overall number of active sites at the electrode surface, the incorporation of In at the surface of Cu-based electrocatalysts limits charge transfer at the electrode surface. The remarkable ability of Cu/In electrodes to suppress HER however is unprecedented, and tackles one of the major hindrances in developing electrodes selective toward CO_2R. It was therefore concluded that a novel approach to improved charge transfer could therefore be address beneath the electrode surface rather than at the electroactive surface.

Though often overlooked for use in electrochemical CO_2 reduction due to its high selectivity toward hydrogen [18] as a result of CO over-binding [19–21], Pt was selected for use in improving electrocatalytic activity of Cu_2O/In electrodes due to its remarkably high conductivity (9.43×10^6 Sm^{-1}). By incorporating high-conductivity materials such as Pt beneath the electrode surface, particularly at points of high resistance such as at the gas diffusion layer, it was anticipated that electrocatalytic activity would be greatly enhanced through the more efficient transfer of charge, resulting in an electrode material both active and selective toward CO_2R.

Herein we examine the effect of Pt deposition beneath the electroactive surface of Cu_2O/In electrodes and present a cutting-edge, activity enhanced tri-metallic electrode through tailored Pt deposition depth. Through electrochemical analysis, we examine novel electrodes in terms of their applications to overcome key challenges within the field of electrocatalysis, examining their performance in terms of 3 key factors: selectivity, activity, and stability. From the results presented herein, we demonstrate a universal method of activity enhancement over previous electrocatalyst designs through Pt incorporation within the GDL, moving one step closer toward producing CO_2 reduction electrocatalysts viable for use on an industrial scale.

2 Experimental Methods

2.1 Preparation of Cu_2O/In/Pt Electrodes

Electrodes were prepared using commercial-grade cuprous oxide (Cu_2O) (Sigma-Aldrich, ≥ 99.99%) deposited on 2.5x2.5 cm carbon paper gas-diffusion electrode support (GDE) (H2315 I2 C6, Freudenberg). Cu-based catalytic ink was prepared using 30 mg Cu_2O dispersed within a 400 μl solution of isopropanol before adding 66 μl nafion perflurated resin (Sigma-Aldrich, 5%Wt.) drop-wise to the solution. The solution was then subsequently sonicated for 10 minutes at room temperature. Cu-based ink was then deposited via painting up to a recommended loading of ≈5 $mgcm^{-2}$, producing an active area of 2 cm^2, suggested in the literature to provide an optimal loading depth in terms of both electrocatalytic activity and selectivity [22]. Catalysts were dried between the painting of each layer at (60^oC 1-3 minutes) and subsequently weighed until achieving the desired loading. It should be noted however that despite the weighing of each electrode following the painting of each additional Cu_2O layer, the loading of the produced catalysts were observed to vary between 4.75 and 5.25$mgcm^{-2}$. Loading values were based solely on the observed weigh values, replicating the method of prior work [22].

Cu_2O/In and Cu_2O/In/Pt electrocatalysts were prepared using an In electroplating method adapted from previously published deposition methods shown to produce Cu_2O/In electrodes highly selective toward CO formation [2,17]. Samples were prepared by injecting an acidified solution (pH 1.72) of 0.05 M $In_2(SO_4)_3$ (Thermo-Scientific, 99.99%) and 0.4 M citric acid (Sigma-Aldrich, ≥99.5%), into an in-house designed deposition cell. As-prepared Cu_2O electrodes were then used as the cathode material, and In foil (Advent Research Materials, 99.999%) as the anode to facilitate the electroplating process. Electro-deposition was carried out over 35 minutes at a fixed current of 0.06 A, with gradually increasing potentials observed ranging from 0.05 V to 1.3 V as a result of the transfer of In cations to the cathode surface.

To produce distinct sub-surface platinum layers, Pt was sputtered using Quorum Q150R ES sputtering machine at selected depths of 8, 5 and 2 μm from the active surface in layers of 10 nm thickness each. Deposition depth was calculated based on Cu loading weight and solution density, through which the approximate quoted depths corresponded to a respective loading of Cu deposited on the catalyst surface (e.g: 8 μm = 0 $mgcm^{-2}$ Cu, 5 μm = 2 $mgcm^{-2}$ Cu and 2 μm = 4 $mgcm^{-2}$ Cu). In each case, Cu_2O was deposited as previously described up to the desired sputtering loading value before depositing Pt, with 8 $mgcm^{-2}$ corresponding to Pt deposition on the GDE layer, then subsequently weighed and painted up to a total loading of ≈5 $mgcm^{-2}$ before finally depositing In.

2.2 Electrochemical Analysis

All electrochemical experiments and measurements were conducted at ambient temperature and pressure using a potentiostat (Metrohm AutoLab PGSTAT302N) and examined using Metrohm Nova 2 software [23]. The flow rate of CO_2 (BOC, 99.9%) was maintained throughout at a constant rate of 15 ml min^{-1} using a designated flow meter (Omega FT-062-09-GL-VN). 1.0 M KOH solution (Thermo Scientific, 85%) was employed throughout both as catholyte and anolyte. In each case, a 3-electrode gas-diffusion electrode (GDE) system based on previously published designs [22] was 3D printed in-house and employed using an Hg/HgO alkaline reference electrode (RE-61AP, Basi, 1.0 M NaOH, 0.098 V vs. SHE) and Pt wire as the counter electrode (Sigma-Aldrich, 7.5 cm). All applied potentials reported were converted to the reversible hydrogen electrode (vs RHE), unless otherwise stated. The incorporation of a GDE electrochemical cell was primarily implemented due to the drastic improvements in catalyst activity as a result of improved CO_2 coverage, with the design posed having previously demonstrated drastic improvements in current

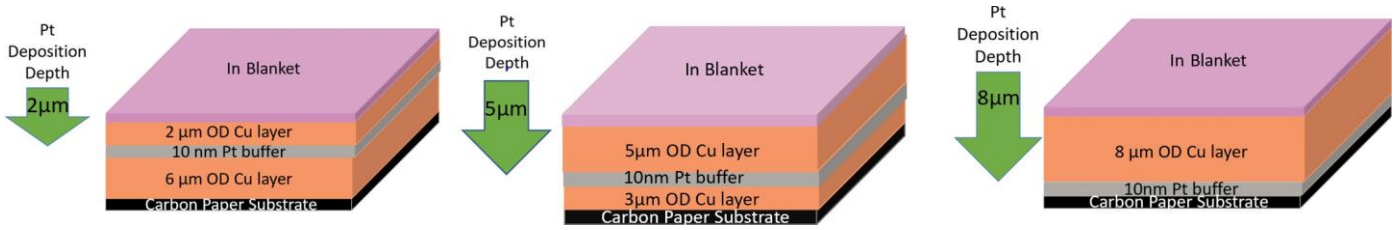

Fig. 1 Conceptual tri-metallic Cu_2O/In/Pt electrocatalyst design, with included Pt sputtering depths.

density of 200 $mAcm^{-2}$ at mild potentials of -1.17 V vs RHE. To ensure a clear separation of cathodic and anode chambers, a cation exchange membrane (CEM) (Fumapem, F-950), minimising recombination reactions to form CO_2 from previously reduced products under potential.

In order to supply a constant supply of fresh catholyte to the cell, a peristaltic pump, designed in-house using smart digital 30 A PwM DC motor remote speed control unit equipped with 4 Gikfun 12 V peristaltic liquid pump dosing pumps, was employed. Its use both ensured homogeneous local pH throughout, as well as to continually remove liquid products, maintaining reaction equilibrium through a continuous supply of fresh electrolyte.

The flow rate of anolyte and catholyte was maintained throughout at 2 ml min^{-1} each, with cathode and anode chambers being connected to their own individual pumping circuit respectively to avoid cross-contamination of oxidised and reduced products.

Electrochemical characterisation of electrocatalysts was performed using a combination of cyclic voltammetry (CV), Chronoamperometry (CA), and electrical impedance spectroscopy (EIS). CVs were carried out in three cycles between -1.5 V and 0.5 V with a scan rate of 50 mV s^{-1} to explore initial electrochemical behaviour of the working electrode, examining both changes in observed current density with potential, in addition to possible changes in CO_2R onset potentials with varying Pt depth.

CO_2RR was carried out via chronoamperometry (CA), with electrical current values being recorded at a range of potentials (-0.5, -0.75, -1.0, -1.25, and -1.5 V vs RHE) over a period of 1 hour in each case. Current values were then standardised against the working electrode surface area (2 cm^2) in each case to calculate the resulting current density (j) and examine electrode stability and activity with prolonged use.

EIS was performed at an AC amplitude of 10 mV over a frequency range of 10 kHz to 0.01 Hz at -0.6 V vs RHE for each electrode. All impedance spectra were analysed and fitted using Nova 2.0 software [23], providing a picture of the interplay between internal catalyst resistivity and double-layer capacitance effects produced during operation. To reduce the impact of sub-surface oxides on individual electrode performance, each electrocatalyst was reduced over a period of 30 minutes at -1.5 V vs RHE prior to EIS examination.

2.3 Product Analysis

Gaseous products were collected during chronoamperometry experimentation from a period of 20 minutes prior to the end of each experiment. Gaseous products were then subsequently analysed via gas chromatography using a Shimazu Tracera GC-2010 gas chromatograph, equipped with flame ionisation- (FID) and thermal conductivity detectors (TCD). A ShinCarbon ST micropacked column 80/100 (Restek) was used to quantify concentrations of permanent gasses and light hydrocarbons present following CO_2 reduction. Samples were stored using air-tight gas bags (Hunan BKMAM, 0.2 L), with gaseous products being extracted from gas bags and injected into the GC using a gas-tight syringe (Hamilton 1000 series, 1 ml) immediately before analysis. Gaseous concentrations were derived via comparison with 5000 ppm Propylene 7 gas mix gas (Boc, propylene 5000 ppm, ethane 5000 ppm, ethylene 5000 ppm, methane 5000 ppm, carbon monoxide 10,000 ppm, hydrogen 10,000 ppm, carbon dioxide balance). The presence of volatile fatty acids (VFA), including formic acid, were analysed quantitatively using Eco IC (Metrohm) ion chromatograph equipped with Metrohm 6.1005.200 column, with a combination of liquid products and depleted catholyte being collected following 1 hour continuous operation under a given potential. Samples were filtered prior to analysis using Fisherbrand non-sterile PTFE syringe filters (13 mm membrane diameter, 0.45 μm pore size) to remove any particulates that may have collected within the extracted electrolyte during experimentation. 2 μl of filtered solution was deposited in a sample vial and diluted using 1.8 μl of DI water. Concentrations were then compared against a formate standard (Sigma-Aldrich, 1000 mg/l ± 5 mg/l to derive formate concentrations.

Following the collection of both gaseous and liquid reduction products, the faradaic efficiencies (FE) for each product were then calculated using Faraday's law [22]

$$FE = \frac{znF}{Q} \quad (1)$$

where F is Faraday's constant (96,500 C mol^{-1}), n is the mass of the desired product in moles, Q denotes the total charge passed, and z is the number of electrons transferred per mole of reactant (e.g. z=8 for the conversion of CO_2 to CH_4). By calculating the respective FEs of each observed reaction product, a clear picture of the the overall selectivity of a given electrode could be produced, providing a clear picture as to any observed effect on electrocatalytic performance with varying Pt depth in regards

specific product formation.

2.4 Characterisation of Cu_2O/In/Pt Electrocatalysts

To examine the crystal composition of all synthesized electrodes, material characterisation was obtained via X-ray diffractometry (XRD), performed using a Rigaku SmartLab SE equipped with Cu X-ray tube (Cu–Kα1; λ =0.154 nm) operated at 40 kV and 50 mA. All scans were produced using a Bragg-Brentano configuration, scanning at a rate of 5 ^{o} per minute. Prior to examination, samples were cut into 0.5×0.7 mm sections and stabilised on 25×75 mm glass slides using double sided tape.

Similarly, X-ray photoelectron spectroscopy (XPS) was performed to determine both the valence states of the cathode, as well its elemental composition at the electroactive surface, using a Kratos Axis Nova XPS spectrometer equipped with a K-Alpha line X-Ray source (225 W) over an area of approximately 300×700 μm.

Finally, microscale characteristics were obtained using Tescan MIRA 3 scanning electron microscope, featuring a high brightness Schottky emitter to produce high resolution images with minimal noise. Electrocatalytic surfaces were examined using back-scattered electrons (BSE) at a working distance of 10 mm at an accelerating beam voltage of 6 kv. Beam spot size was minimised in all cases to examine sharp topographical features. Samples in each case were handled using tweezers cleaned using propanol and adhered to the sample platin via 3M scotch tape. In each case samples were pumped down overnight to reach the required pressure for analysis.

Energy Dispersive X-ray Spectroscopy (EDS) functionality from Oxford instruments (X-Max), enabled further analysis through the examination of atomic surface compositions. EDS was collected at a working distance of 15 mm using an accelerating beam voltage of 6 kV, ensuring a high resolution was maintained when producing EDS mapping data. To ensure minimal background noise, EDS was performed under dark conditions. Samples were cut into sections 1×1 cm and immobilised on 12.5 mm diameter aluminium studs using carbon adhesive discs. Prepared samples were subsequently screwed in place to ensure high stability when examining electrocatalyst morphology under high magnification.

3 Results and Discussion

3.1 Characterisation of Tri-Metallic Electrocatalysts

To examine the potential impact of Pt at various depths beneath the electroactive surface, Cu_2O/In/Pt electrodes were prepared at a range of Pt depths of 2, 5 and 8 μm. In each case, Pt was deposited via sputtering up to a thickness of 10 nm.

EDS images shown in figure 2 confirm the presence of Pt following deposition through the observed formation of an even coverage of ultra-thin Pt layers when deposited both at the GDL (8 μm). Similarly, the formation of a Pt layer can be observed on Cu_2O (2 μm) post-sputtering, indicating the successful incorporation of within the electrode.

To minimise the impact of HER on the selectivity of produced electrodes, In was electro-deposited at the active surface region prior to electrochemical experimentation. Electro-deposition has proven to be a highly reliable method of producing bi-metallic composite electrocatalysts [2,24–26]. Due to its widespread use and simplicity of its deposition method, the electro-deposition of In was introduced as a reliable method of In deposition.

The results of electro-deposition of In on Cu_2O/Pt electrodes for the case of 2 μm Pt can be observed in figure 3. SEM images shown in figure 3 indicate a clear alteration of electrode surface topology following In deposition. The sharp, angular micro-grains of deposited Cu_2O prior to deposition appear largely replaced by smooth, irregular surface structures, likely produced through surface restructuring effects during the In deposition process as a result of both In adhesion and the reduction of Cu_2O under potential.

EDS mapping data shows similar distribution regions for both Cu and O across the surface, indicating the catalytic surface to primarily be composed of copper oxide groups. This oxidised copper is likely Cu_2O due to the high ratio of copper to oxygen observed in figure 3, as well as the strong Cu_2O signals observed via XRD both pre- and post-deposition. EDS results further show that In, for the most part, deposits evenly across the Cu_2O surface, though demonstrates stronger signals near ridge-like regions where the electrode surface forms micro-folds and crevasses. This surface coverage of In suggests a high probability of HER suppression in favour of CO_2R, with any deviation from prior results likely to occur as a result of variations in surface morphology as opposed to compositional variation. EDS spectra in figure 3 additionally indicated no sign of Pt present on the electrode surface both before and after In deposition, implying any observed changes in performance would be driven by the surface characteristics of Cu_2O/In, enhanced by interactions with Pt bulk layers.

X-ray diffraction (XRD) results of Cu_2O/In/Pt with 2 μm Pt appear to support this hypothesis, showing no significant presence of Pt following the reduction of the catalyst during the electroplating process, instead detecting almost exclusively Cu and Cu-oxide groups. This further suggests that Pt has limited interaction with adsorbates at the surface, but rather influences the electrocatalyst from sub-surface and bulk regions through charge-transfer effects. XRD results additionally support the idea of surface recombination during electroplating as a result of the reduction of Cu_2O, with post-deposition spectra demonstrating clear Cu signals associated with the (111) and (200) facets. Pre-deposition XRD spectra however, demonstrates no signals for pure Cu, suggesting a clear reduction of Cu-oxide species under potential.

Due to the observed changes in morphology likely linked to the reduction of Cu-oxides at the electrode surface, SEM images were collected both prior to, and post catalysis. The collection of such images allowed for a clear examination of possible recombination effects resulting from long-term use of Cu_2O/In/Pt electrodes under potential. Post-catalysis images of Cu_2O/In/Pt 2 μm Pt shown in figure 4 demonstrate a considerable change in surface morphology, indicating clear alterations in surface characteristics following prolonged use.

Following 24 hours of continuous operation at -1.5 V vs RHE in 1.0 M KOH electrolyte Micro-spindle protrusions up to 3 μm in length can be observed, indicating clear surface restructuring effects as a result of Cu_2O/In/Pt electrodes being subjected to long-

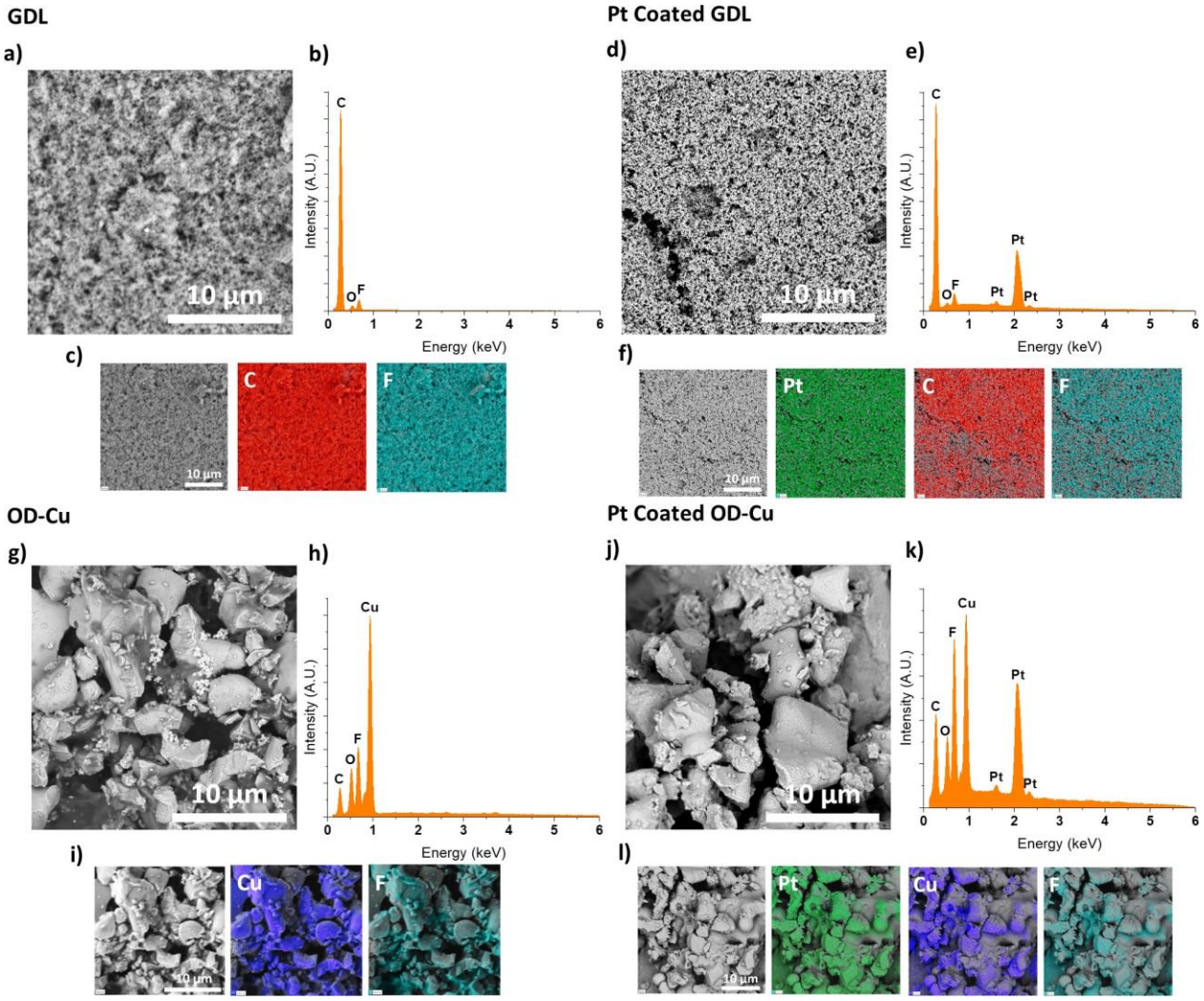

Fig. 2 Pre- and post-Pt sputtering characterisation of the GDL and Pt interfacial layers of Cu_2O/In/Pt electrodes. a) Pre-deposition SEM image of the GDL, b) EDS spectra and c) EDS mapping of pre-Pt deposition electrode surface. d) Post-deposition SEM image of the GDL taken prior to further OD-Cu deposition (8 μm), and its corresponding e) EDS spectra and f) EDS map. g) Pre-deposition SEM image of the OD-Cu electrode, h) EDS spectra and i) EDS map of pre-Pt deposition electrode surface. j) Post-deposition SEM image of the Cu_2O/In/Pt electrode taken at the Pt interfacial layer prior to further OD-Cu deposition (2 μm), and its corresponding k) EDS spectra and l) EDS map.

term CO_2RR conditions. Observed changes in surface roughness resulting from micro-spindle formation likely result in a greater overall surface area, likely accounting for the gradual increase in electrocatalyst activity through the formation of additional active sites. This gradual increase in surface roughness could also account for increases in HER over prolonged use, with high-surface area electrodes providing a greater quantity of low-coordination active sites demonstrated previously to promote HER [27].

Due to the drastic changes in surface morphology observed following CO_2R, XPS analysis methods were employed to examine possible changes in the chemical composition of the electrode surface, the results of which can be seen in figure 5.

XPS analysis of the electrode shows a distinct change in the oxidation state of the electrode surface following the deposition of In. Prior to deposition, Cu_2O/Pt shows a strong Cu^{2+} satellite peak associated with the presence of CuO located at 942.3 eV [28,29], further supporting evidence of the reduction of Cu oxides under potential.

Peak fitting of Cu_2O/Pt spectra additionally detects the presence of Cu_2O/ Cu at 933.2 eV [30,31] broadened by a neighbouring CuO peak located at 936.2 eV [32]. Following the electro-deposition of In however, CuO signals appear notably reduced in comparison with that of Cu_2O/ Cu, suggesting a reduced OD-Cu surface being produced during the deposition process. This Reduction can further be observed to a lesser extent when examining Cu_2O/In/Pt electrodes following electrocatalysis, indicating possible changes in surface structure during the reduction process as OD-Cu shifts toward a lower oxidation state. This would seem to suggest that the observed changes in surface roughness are indeed linked to the reduction of Cu-oxides following its exposure to CO_2R conditions.

Following on from the examination of changes in Cu oxidation states, XPS analysis was employed to examine In surface composition both prior to-, and post- catalysis. Though undetectable

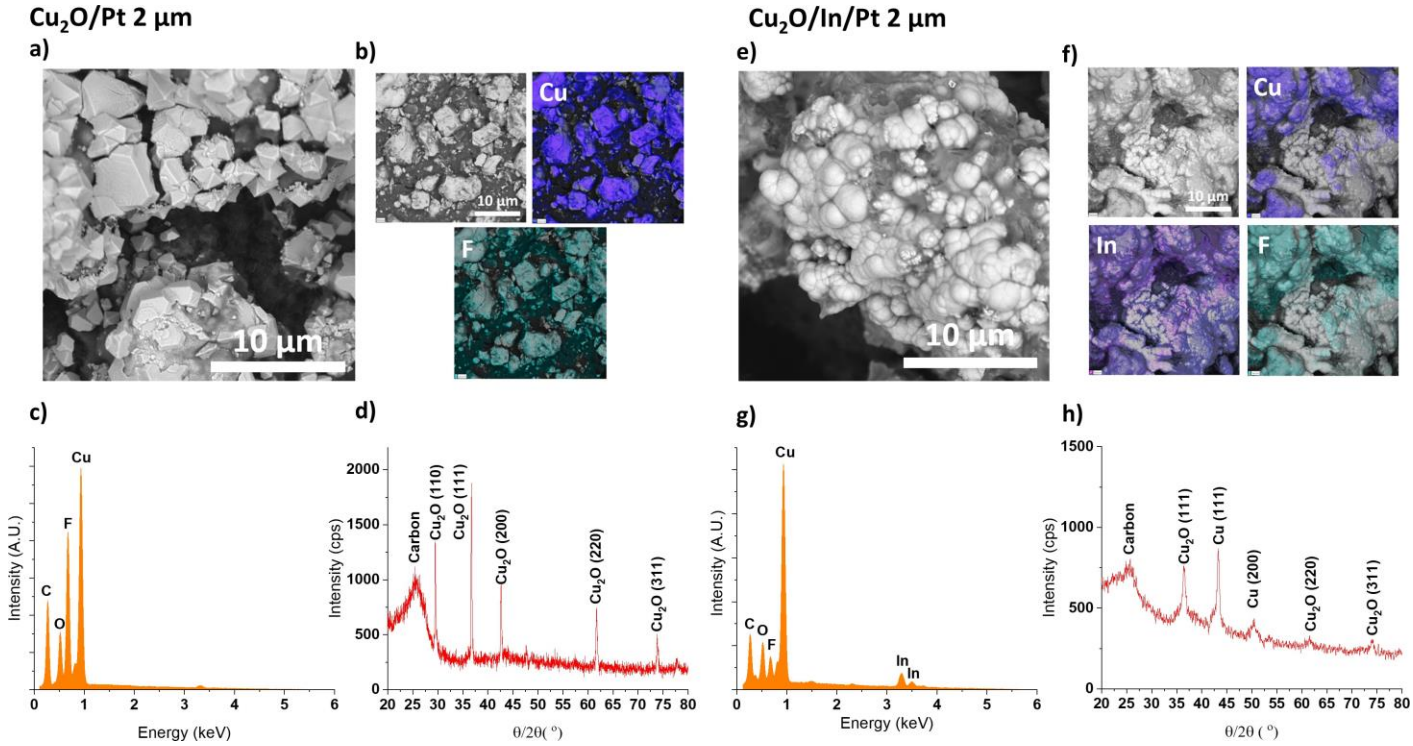

Fig. 3 Comparison of Cu_2O/In/Pt 2 μm electrodes pre- and post In electroplating. a) SEM image of pre-electroplated electroactive surface region, b) EDS map of observed elements pre-electroplating, c) pre-electroplated EDS spectra, and d) pre-indium deposited XRD spectra. e) SEM image of post-electroplated Cu_2O/In/Pt, f) post-electroplated EDS map, g) EDS spectra of post=In deposited Cu_2O/In/Pt, and h) XRD spectra following In deposition.

via XRD, x-ray photoelectron spectroscopy (XPS) spectra in figure 5 confirms its presence on the surface of Cu_2O/In/Pt following deposition due to distinct photoelectronic peaks in the In3d spectrum. Analysis of the 445.7 eV peak was assigned to that of the $In3d_{5/2}$ peak of In_2O_3. A secondary peak assigned to In_2O_3 in the $In3d_{5/2}$ region, was also observed at 447 eV following peak fitting [33,34].

Post-electrocatalysis results following 24 hours continuous operation at -1.5 V vs RHE in 1.0 M KOH electrolyte additionally show a notable shift in the observed In peaks, with In_2S_3 shifting toward a lower binding energy of 445 eV, believed to be that of $In(OH)_3$ [35,36]. This shift likely occurs as a result of interactions between the In_2O_3 deposits and water within the electrolyte solution [37].

3.2 Electrochemical Performance of Cu_2O/In/Pt

Cu_2O/In/Pt prepared at a range of Pt deposition depths (8 μm, 5 μm and 2 μm), as well as the precursor Cu_2O and Cu_2O/In catalysts, were examined via electrochemical CO_2 reduction over a range of potentials (-0.5 to -1.5 V vs RHE). To facilitate the CO_2RR, a 3-electrode GDE cell was used with 1 M KOH electrolyte (pH 13.92) based on the success of prior studies [17,22]. This combination of both GDE cells and highly alkaline electrolyte help to facilitate improved mass transport of CO_2, improving general reaction kinetics. [38,39]

To assess possible changes in electrochemical performance, each electrode was examined using cyclic voltammetry (CV), investigating each electrocatalyst under both N_2 and CO_2 enriched atmospheres, with gasses being bubbled through the GDE cell at rates of 20 ml min^{-1} and 15 ml min^{-1}, respectively. CV experiments were performed across a potential range of 0.5 to -1.5 V vs RHE.

CV results appear to demonstrate a general improvement in catalytic activity for Cu_2O/In/Pt electrodes when compared with Cu_2O/In. For both the case of N_2 and CO_2 enriched atmospheres, Cu_2O/In/Pt electrodes demonstrate a clear improvement in observed current densities over that of Cu_2O/In, achieving values comparable to that of OD-Cu for the case of 8 μm deposited Pt Cu_2O/In/Pt. Upon closer examination, a clear trend can be observed relating Pt deposition depth to observed current densities. In each case, catalysts demonstrated a gradual increase in current density as Pt was deposited closer to the base of the electrode, i.e: 8 μm > 5 μm > 2 μm > Cu_2O/In. This would suggest Pt is therefore most effective in improving electrocatalyst activity when deposited closer to the base of the electrode, as opposed to near the active surface. Due to its distance from the electroactive surface for the case of 8 μm deposited Cu_2O/In/Pt, this would suggest Pt influences the electrode through bulk charge transfer effects, as opposed to influencing adsorption characteristics. Due to a similar trend observed for the observed onset potentials of Cu_2O/In/Pt electrodes to that of Cu_2O/In and OD-Cu, this would likely appear to be the case. It should be noted however that one key difference observed between Cu_2O/In and Cu_2O/In/Pt electrodes is that of the reduction peaks observed during exper-

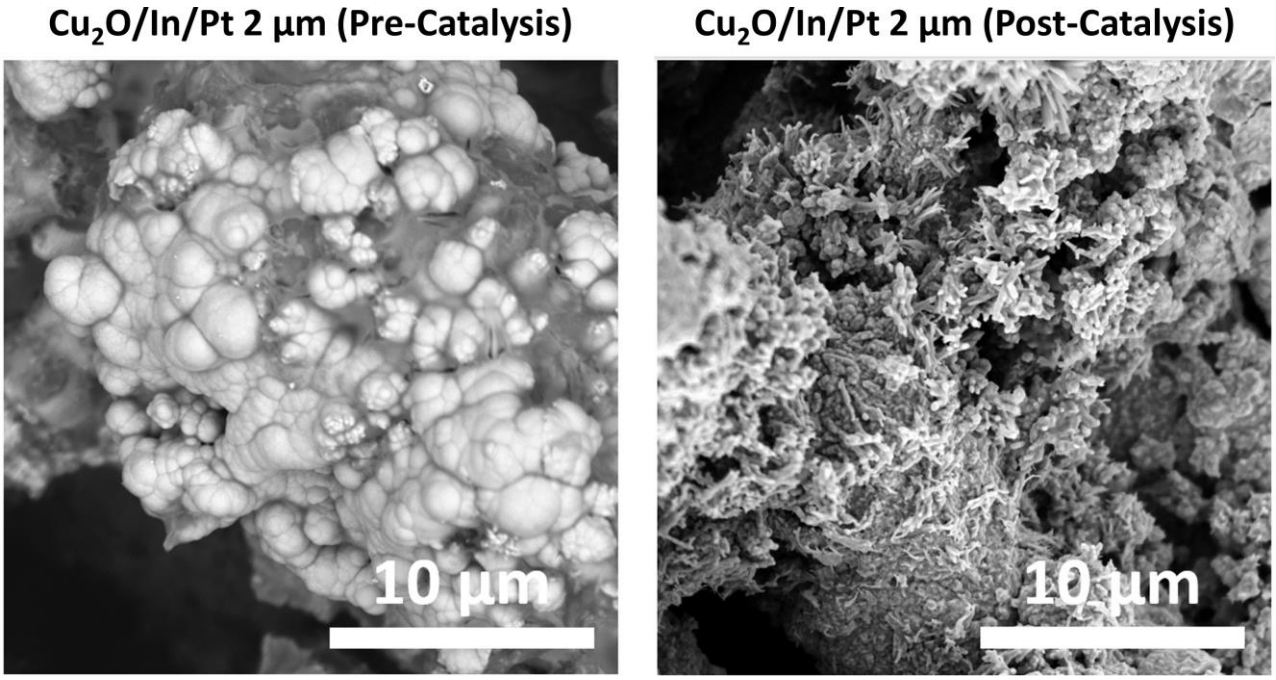

Fig. 4 SEM images of Cu_2O/In/Pt 2 μm electrodes pre- and post-catalysis.

imentation. Prominent in both cases, though more pronounced when conducting scans in N_2 atmosphere, the reduction peaks of Cu_2O/In/Pt electrodes are considerably larger than for that of their counterparts. Such changes are likely the result of enhanced HER activity, with greater quantities of hydrogen being produced as charge transfer is more greatly improved across the electrocatalyst.

To assess both the stability and activity of produced electrodes, in addition to their overall effectiveness in reducing CO_2 in aqueous media, Cu_2O/In/Pt electrodes were examined via chronoamperometry. To compare changes in electrode performance, OD-Cu and Cu_2O/In standards were examined under identical conditions.

Each electrocatalyst was tested across a potential range of -0.5 V vs RHE to -1.5 V vs RHE under ambient temperature and pressure. Each catalyst was tested for 1 hour at each potential before increasing the potential by a step of -0.25 V, resulting in each electrode being examined for a total of 5 hours. Prior to each step increase of potential, electrolyte was purged from the electrochemical cell for analysis, and a fresh supply of 1.0 M KOH was provided to both anode and cathode chambers to ensure a ready supply of charge carriers within the CO_2 reduction cell. Regardless of both potential, and Pt deposition depth, Cu_2O/In/Pt electrodes demonstrated generally stable current densities for 5 hours across the various potentials, as shown in figure 6. At more negative potentials (> -1.25 V vs RHE) however, a gradual increase in current density can be observed for 8 μm deposited Cu_2O/In/Pt. Due to both the large current densities observed for 8 μm Cu_2O/In/Pt, and the previously observed surface restructuring effects observed for produced electrodes under potential, it appears highly probable that such increases occur as a result of the formation of a greater number of active sites under CO_2 reduction conditions, with more negative potentials seemingly driving the restructuring process at an accelerated rate.

Based on the general trend of recorded CA results, it seems to suggest, despite the added complexity of the electrocatalyst, that tri-metallic electrodes offer highly stable operation across a wide potential window. Furthermore, a consistent trend in enhanced activity of Cu_2O/In/Pt electrodes over Cu_2O/In above -1.5 V vs RHE was observed. In particular, Cu_2O/In/Pt electrocatalysts for which Pt was deposited at 8 μm below the electrode surface, i.e. interspersed within the carbon paper backing, consistently exhibit the greatest current densities, achieving -204 $mAcm^{-2}$ at -1.5 V vs RHE. This increased catalytic activity likely suggests Pt enhances charge transfer even when deposited within the catalyst bulk, with the most prominent effects occurring where Pt is deposited on the GDL. This appears to strongly agree with CV results, supporting the idea of enhanced electrode performance through Pt incorporation within the GDL.

EIS results shown in figure 7, appear to agree with this hypothesis. By examining each electrode material at -0.6 V vs RHE, the obtained impedance spectra demonstrates a clear trend through the incorporation of Pt. By depositing Pt within the GDL, Cu_2O/In/Pt electrocatalysts demonstrated a notable decrease in cell resistance, likely a result of a reduced internal resistance of the electrocatalyst through the inclusion of Pt, resulting in improved charge transfer throughout the electrode.

Though this effect could still be observed to a certain degree with both 5 μm and 2 μm Cu_2O/In/Pt electrodes, its potency compared with that of the 8 μm case appears reduced, resulting in both increased reactance, as well as a larger solution resistance. Such changes are likely due to a reduced contact between the deposited Pt layers and the GDL, resulting in an EIS profile similar to that of Cu.

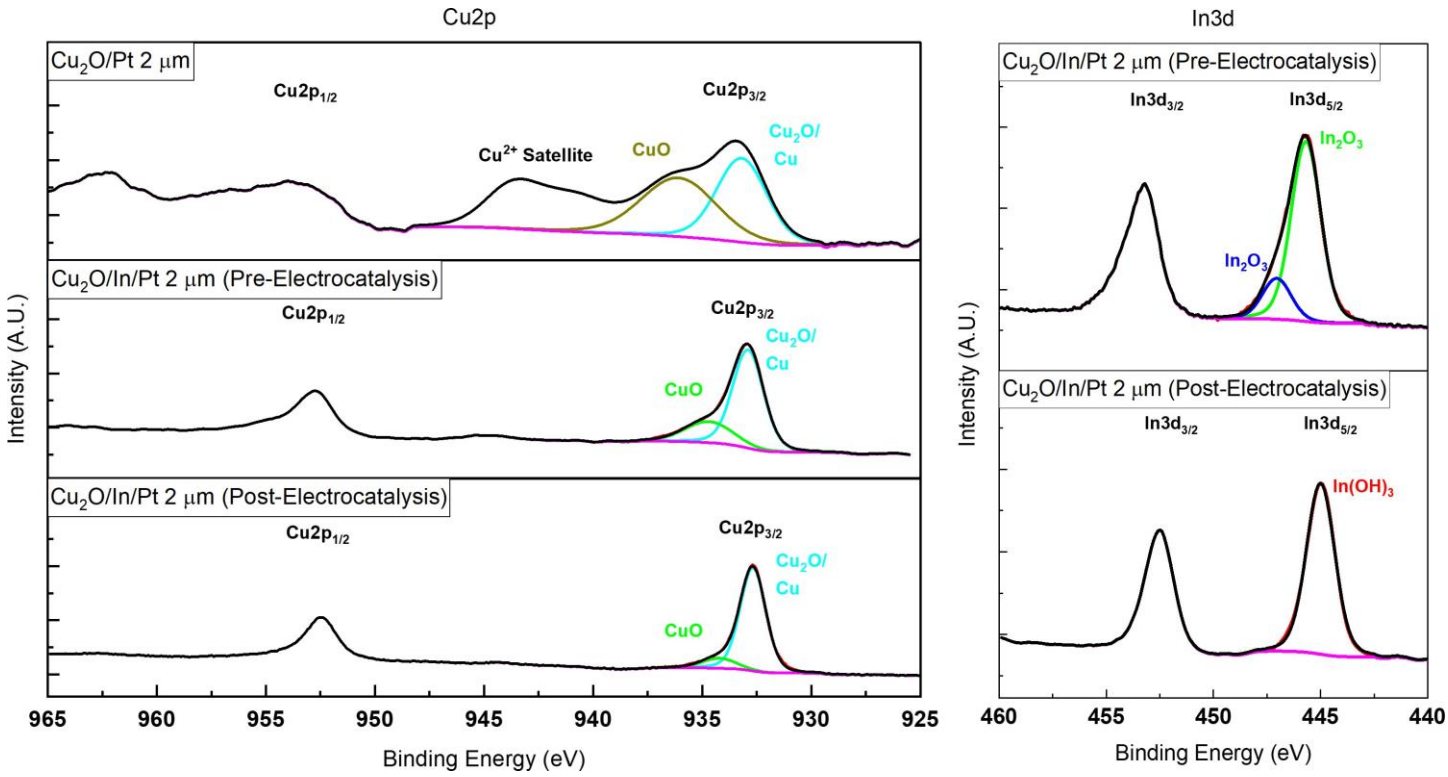

Fig. 5 High-resolution XPS spectrum of Cu2p for Cu_2O/Pt 2 μm (top), Cu_2O/In/Pt 2 μm (pre-electrocatalysis) (middle), and Cu_2O/In/Pt 2 μm (Post-electrocatalysis) (bottom). In3d XPS spectra examined for Cu_2O/In/Pt 2 μm (pre-electrocatalysis) (top), and Cu_2O/In/Pt 2 μm (Post-electrocatalysis) (bottom).

Results obtained for the electrochemical reduction of CO_2 using Cu_2O/In/Pt electrodes following electrolysis demonstrate a notable decrease in HER selectivity at -0.5 V vs RHE when compared with OD-Cu. HER selectivity decreased from 31.5% for OD-Cu, down to 9.2% for the case of Cu_2O/In/Pt 8 μm, demonstrating a similarly low selectivity toward HER as that of Cu_2O/In (8.1%) at the same potential. This decrease in HER was accompanied by a drastic increase in CO formation, up to a maximum FE of 85.9% for Cu_2O/In/Pt 8 μm. At more negative potentials however, CO selectivity decreased in favour of hydrogen, and carbonaceous products such as methane and ethylene. The overall selectivity of the Cu_2O/In/Pt electrodes beyond -0.5 V vs RHE appears to demonstrate increased HER selectivity, with a gradual improvement in CH_4 formation over OD-Cu from potentials more negative than -1.0 V vs RHE. By comparing the FE values with observed current densities and EIS profiles in figure 7, this would appear to demonstrate a gradual reduction in HER as Pt was deposited at more shallow depths within the catalyst bulk. This would suggest improved charge transfer could also provide one possible explanation of the observed trend in increased H_2 formation for 8 μm Cu_2O/In/Pt electrodes when compared with that of 2 μm and 5 μm. Though Pt appears to offer no direct impact on product selectivity via alterations in surface adsorption characteristics, the knock-on effect of its improved electrode activity could account for such increases in HER selectivity. HER has often been observed to be more kinetically favourable than CO_2RR [40], with theoretical equilibrium potentials for HER occurring at 0 V vs RHE as opposed to -0.10 V for CO formation. Due to such properties, it seems probable that with increased charge transfer through Pt doping, the formation of H_2 is subsequently enhanced to a greater extent than the formation of less kinetically favourable products. This hypothesis could be further supported by a 2013 work by Reske et al. [41], suggesting Pt requires a distance of < 15 nm from the electrode surface through which it can tune C_{2+} product selectivity, suggesting changes in selectivity in this case to likely be a result of the abundance of charge as opposed to any direct impact on adsorption characteristics resulting from Pt's incorporation within the electrocatalyst bulk.

By comparison with SEM results, this could also suggest increased HER selectivity occurs as a result of micro-spindle formation, with greater charge transfer likely facilitating a more rapid reduction of OD-Cu at the electrode surface to form a greater volume of hydrophilic active sites, resulting in greater hydrogen selectivity.

Beyond observed trends in hydrogen formation, C_2H_4 selectivity was also observed to decrease on Cu_2O/In/Pt electrodes when compared with OD-Cu, instead producing small quantities of CH_4, particularly at more negative potentials. This increase in CH_4 formation is likely a result of the more negative potentials induced [42]. The formation of CH_4 has also previously been demonstrated to preferentially form on tightly bound Cu (111) crystal facets, particularly at more negative potentials [43]. By contrast, C_2H_4 has been shown to preferentially form on both flat Cu(100) facets, as well as step sites such as on the (110) facet. This could suggest the formation of CH_4 on Cu_2O/In/Pt electrodes could also be due to an increased proportion of (111) facets present on the

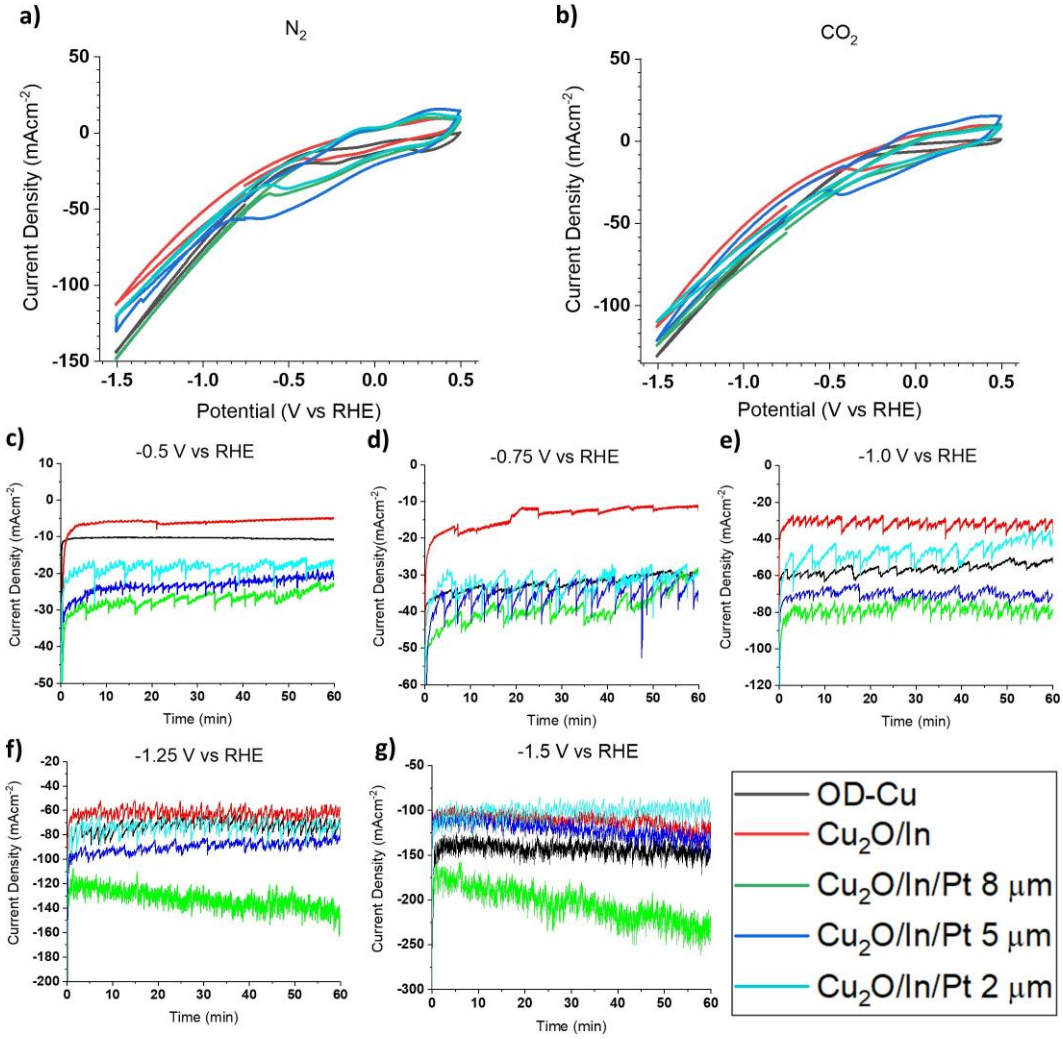

Fig. 6 Cyclic voltammetry profiles of Cu_2O/In/Pt electrodes at varying Pt sputtering depth under a) N_2 and b) CO_2 atmospheres. Additionally, chronoamperometry results for Cu_2O/In/Pt electrodes with varying Pt deposition depth at varying potentials versus RHE c) -0.5 V, d) -0.75 V, e) -1.0 V, f) -1.25 V and g) -1.5 V, respectively.

surface. Based on the strong signals for both Cu_2O and Cu (111) facets observed via XRD analysis, this would support this hypothesis, as large quantities of (111) facets would likely improve CH_4 selectivity on Cu_2O/In/Pt electrodes. Due to the small area examined via XRD however, this facet-dependent hypothesis appears unlikely as it is not representative of the entire electrode, suggesting increased CH_4 formation to likely be a result then of both more negative potential and the formation of low-coordination Cu surface protrusions to facilitate the hydrogenation of carbonaceous intermediates.

Prior studies in Cu_2O/In electrocatalysts have often demonstrated high suppression of HER in favour of CO formation by blocking HER active sites [2,17]. Results shown in figure 7 however demonstrate a considerable drop in performance below -0.5V vs RHE. SEM images in figure 4 demonstrate a considerable change in the electrocatalytic surface structure following CO_2 reduction, suggesting this increase in HER may come as a result of an altered surface structure. HER has previously been demonstrated to preferentially occur at regions of low Cu co-ordination [2,44]. As the structure of Cu_2O/In/Pt electrodes changes to form higher surface area micro-spindles, it may also increase the proportion of defect sites present on the the electrode surface.

To examine the prolonged performance of Cu_2O/In/Pt, stability tests were performed for the case of ≈2 μm Pt depth over a period of 24 hours at -1.5 V vs RHE, with gaseous and liquid products being extracted on an hourly basis for analysis. Results shown in figure 8 show the 3-point average of the partial current densities of gaseous and liquid products collected throughout the experiment.

Over 24 hours continuous use, Cu_2O/In/Pt shows remarkable stability despite the incorporation of 3 metal centres, reducing CO_2 with an observed average current density of -113 $mAcm^{-2}$ throughout. During stability testing, the observed total current density can be seen to gradually increase over the full 24 hours, from an initial value of -104 $mAcm^{-2}$ to -120 $mAcm^{-2}$. During this time, HER partial current densities demonstrate a similar

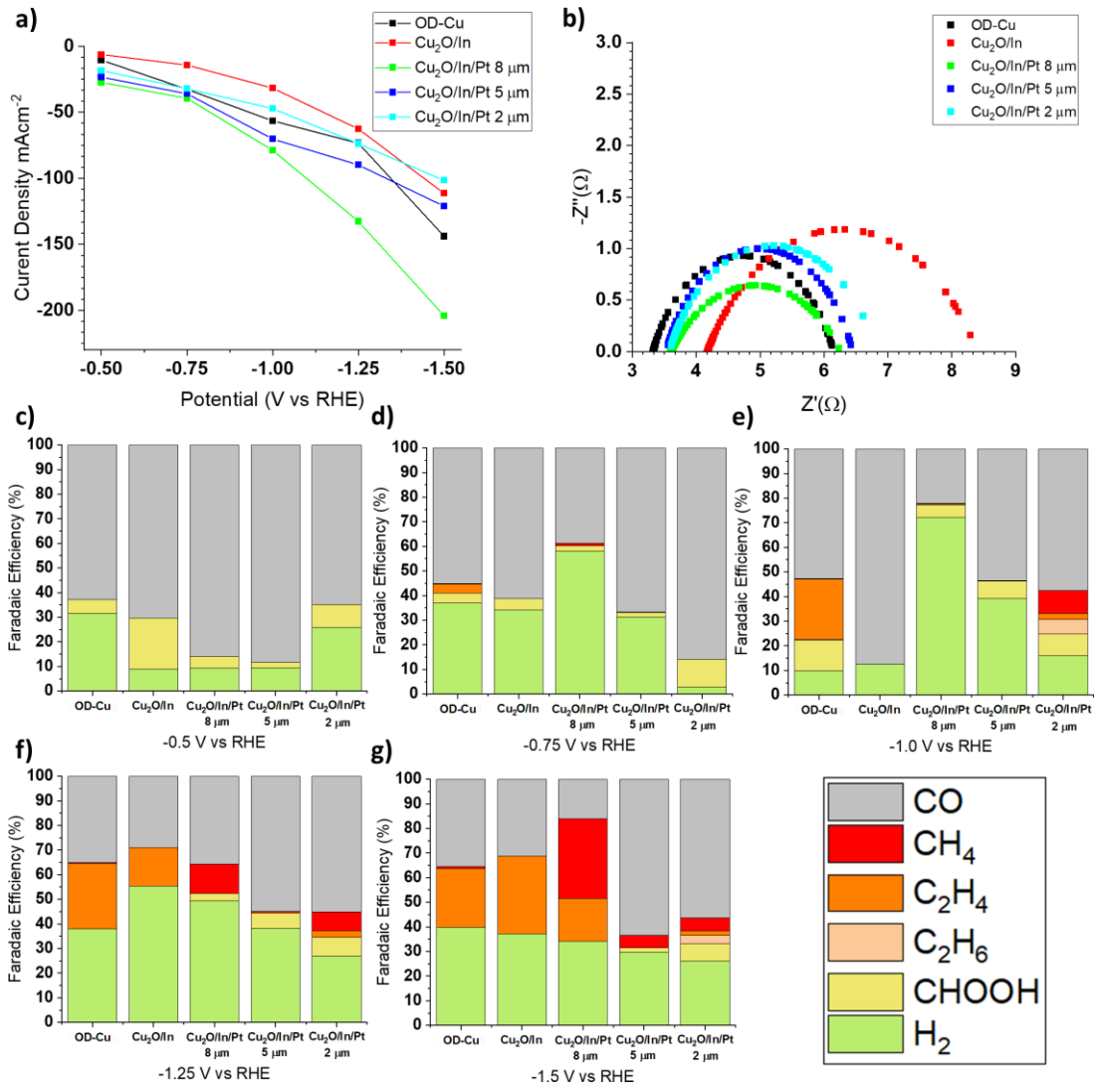

Fig. 7 a) Observed average current densities observed for OD-Cu, Cu_2O/In, and Cu_2O/In/Pt electrodes following 1 hour continuous operation at varying potential, and b) Electrical Impedance Spectroscopy of OD-Cu, Cu_2O/In and Cu_2O/In/Pt electrocatalysts with varying Pt sputtering depth, recorded at -0.6 V vs RHE. Normalised Faradaic efficiencies for Cu_2O/In/Pt electrocatalysts at various potentials c) -0.5 V, d) -0.75 V, e) -1.0 V, f) -1.25 V, and g) -1.5 V vs RHE.

trend, increasing from -47.1 $mAcm^{-2}$ within the first 3 hours to -60.9 $mAcm^{-2}$ by the final stages of the experiment.

By contrast, partial current densities for CO_2 reduction demonstrate a near constant performance, with the observed partial current density of CO beginning at -43.6 $mAcm^{-2}$ and ending at -44.2 $mAcm^{-2}$. It should be noted however that CO partial current densities demonstrated a gradual increase within the first 9 hours of operation, achieving a peak partial current density of -72.7 $mAcm^{-2}$ before gradually decreasing over the following 15 hours. HER formation appears to be inversely proportional to this trend, gradually being suppressed over 9 hours before reaching a minimum current density of -21.8 $mAcm^{-2}$ and demonstrating a gradual increase in partial current density from that point onward.

Such trends would suggest complex mechanistic effects taking place throughout the long-term operation of the electrocatalyst. Due to the lack of impact of Pt on surface characteristics, as demonstrated previously, this would imply that changes selectivity during the 24 hour period are limited to electronic and morphological effects introduced predominantly by Cu and In. Examination of post-use XPS data indicates a gradual reduction of the OD-Cu layer, whilst post-catalysis SEM images show a clear restructuring of the electrode surface to form high surface area micro-spindles. This would seem to suggest then that the restructuring of the electrode under potential, driven by the reduction of Cu oxides, results in the gradual formation of a greater number of active sites, accounting for the gradual increase in current density. Changes in selectivity then likely occur as a result of this restructuring, as prior studies have previously observed strong ties between the selectivity of H_2 and CO formation with increased

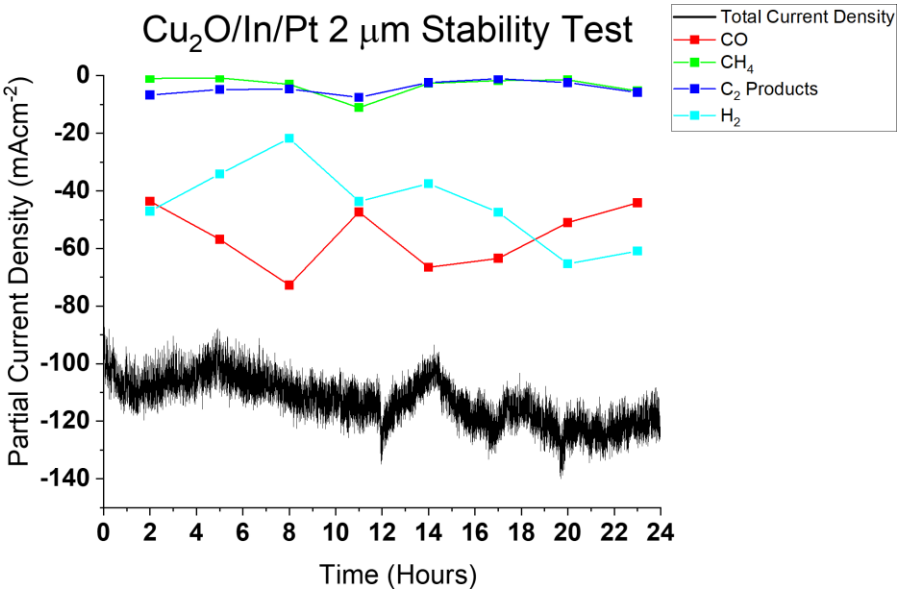

Fig. 8 Chronoamperometry profile of 2 μm Pt depth Cu_2O/In/Pt electrode over 24 hours active use at -1.5 V vs RHE in 1 M KOH electrolyte.

surface area and number of defect sites [27]. It appears likely then, that as the active surface area is initially increased, CO formation is largely promoted, with In ensuring HER remains suppressed, with more prolonged use however, HER increases as a result of the gradual growth of Cu micro-spindles, spreading the protective In layer thinner, gradually reducing its effectiveness as more Cu rich defect sites are produced highly active toward H_2 formation. Cu_2O/In/Pt electrodes therefore indicate a stable activity over 24 hours, though demonstrate a gradual shift in product selectivity as OD-Cu reduces under potential to produce a greater proportion of HER active sites.

Unlike H_2 production, the formation of C_{2+} products remains at a near constant partial current density of -4.45 $mAcm^{-2}$ throughout. This low current density is likely a result of the surface properties of Cu_2O/In/Pt, which strongly mimic its Cu_2O/In counterpart. Prior studies by Rasul et al [1] and Xiang et al [17] have demonstrated a preference for Cu_2O/In electrodes to form CO over C_{2+} products. This has previously been attributed to the nature of the CO* intermediate. CO* dimerization is the rate-determining step in the formation of C_{2+} products [45–49]. CO formation rather, occurs as a result of the desorption of the bound CO* intermediate. This would seem to indicate a reduced binding energy of CO*, preventing the formation of C-C bonds at an appreciable rate. This further suggests a limited interaction by Pt on catalytic surface activity, as Pt has previously demonstrated strong CO binding, often resulting in the poisoning of the electrode, producing predominantly H_2 [21].

4 Conclusions

Novel tri-metallic Cu_2O/In/Pt electrodes examined based on Pt deposition depth within the electrode. Results demonstrate improved current densities of -204 $mAcm^{-2}$ due to improved charge transfer through Pt incorporation within GDE layers. This incorporation of Pt within the GDE overcomes a key limitation in prior Cu_2O/In electrodes, increasing overall catalytic activity by 183%. Tri-metallic electrodes demonstrate no clear increase in the selectivity toward C_{2+} products, however demonstrate a tuneable HER selectivity range as a result of tailored charge transfer effects with Pt deposition depth. This likely suggests a limited interaction between Pt and the active Cu_2O/In surface in terms of tuning CO* binding energies, but rather influences the system through sub-surface electronic and charge transfer effects. Additionally, despite the increased complexity of the electrocatalytic system, Cu_2O/In/Pt electrodes demonstrate remarkable stability over a 24 hour period, with a gradual increase in catalytic activity observed as a result of surface restructuring effects under potential.

The incorporation of interfacial Pt layers within prior electrocatalyst designs provides an interesting area of study, both in terms of examining changes in their electrochemical behaviour, as well as further optimising the catalytic performance to provide cost-effective methods of CO_2 recycling to value-added chemicals and fuels from green house gasses. By incorporating high-conductivity GDE contact layers, future electrocatalyst designs may move one step closer in terms of meeting the required activity, selectivity, and stability goals required to produce industry-grade CO_2 reduction catalysts capable of producing value added chemicals and fuels. Further development of this work could include the examination of Pt within nano-scale depths from the electrode surface to examine more prominent electrochemical effects at the active surface, as well as examining the resulting impact of Pt incorporation within high surface area electrodes incorporating nano-particle structures due to their high selectivity toward multi-carbon products [50].

Author Contributions

Ian Brewis: methodology, data curation, investigation, formal analysis, writing - original draft. Sankeerthana Bellamkonda: for-

mal analysis, project administration, writing - review and editing. Venkateswara Rao Gedela: data curation. investigation, resources. Rana-Faisal Shahzad: resources, writing - review and editing. Abdesslem Jedidi: supervision Shahid Rasul: supervision, conceptualization, methodology, fromal analysis, funding acquisition, resources, validation.

Conflicts of interest

The authors declare no conflicts of interest.

Acknowledgements

This work was supported by the Engineering and Physical Sciences Research Council [grant number EP/S023836/1]

Notes and references

1 S. Rasul, D. H. Anjum, A. Jedidi, Y. Minenkov, L. Cavallo and K. Takanabe, *Angewandte Chemie - International Edition*, 2015, **54**, 2146–2150.

2 A. Jedidi, S. Rasul, D. Masih, L. Cavallo and K. Takanabe, *Journal of Materials Chemistry A*, 2015, **3**, 19085–19092.

3 P. K. Sharma, S. Rasul, D. Li and H. Y. Eileen, *Materials Reports: Energy*, 2023, 100196.

4 D. T. Whipple and P. J. Kenis, *Journal of Physical Chemistry Letters*, 2010, **1**, 3451–3458.

5 J. Durst, A. Rudnev, A. Dutta, Y. Fu, J. Herranz, V. Kaliginedi, A. Kuzume, A. A. Permyakova, Y. Paratcha, P. Broekmann and T. J. Schmidt, *Chimia*, 2015, **69**, 769–776.

6 J. P. Jones, G. K. Prakash and G. A. Olah, *Israel Journal of Chemistry*, 2014, **54**, 1451–1466.

7 P. Zuman, *Advances in Colloid and Interface Science*, 1981, **14**, 282–283.

8 Y. Y. Birdja, E. Pérez-Gallent, M. C. Figueiredo, A. J. Göttle, F. Calle-Vallejo and M. T. Koper, *Nature Energy*, 2019, **4**, 732–745.

9 I. Brewis, R.-F. Shahzad, R. W. Field, A. Jedidi and S. Rasul, *Discover Chemical Engineering*, 2022, **2**, 2.

10 C. Peng, S. Yang, G. Luo, S. Yan, M. Shakouri, J. Zhang, Y. Chen, W. Li, Z. Wang, T.-K. Sham *et al.*, *Advanced Materials*, 2022, **34**, 2204476.

11 Y. C. Li, Z. Wang, T. Yuan, D.-H. Nam, M. Luo, J. Wicks, B. Chen, J. Li, F. Li, F. P. G. De Arquer *et al.*, *Journal of the American Chemical Society*, 2019, **141**, 8584–8591.

12 T. T. Hoang, S. Verma, S. Ma, T. T. Fister, J. Timoshenko, A. I. Frenkel, P. J. Kenis and A. A. Gewirth, *Journal of the American Chemical Society*, 2018, **140**, 5791–5797.

13 N. Furuya, T. Yamazaki and M. Shibata, *Journal of Electroanalytical Chemistry*, 1997, **431**, 39–41.

14 Q. Zhou, X. Tang, S. Qiu, L. Wang, L. Hao and Y. Yu, *Materials Today Physics*, 2023, **33**, 101050.

15 A. Vasileff, X. Zhi, C. Xu, L. Ge, Y. Jiao, Y. Zheng and S. Z. Qiao, *ACS Catalysis*, 2019, **9**, 9411–9417.

16 S. Sarfraz, A. T. Garcia-Esparza, A. Jedidi, L. Cavallo and K. Takanabe, *ACS Catalysis*, 2016, **6**, 2842–2851.

17 H. Xiang, S. Rasul, B. Hou, J. Portoles, P. Cumpson and E. H. Yu, *ACS Applied Materials & Interfaces*, 2020, **12**, 601–608.

18 Y. Hori, H. H. I. Wakebe, T. Tsukamoto and O. Koga, *Electrochimica Acta*, 1994, **39**, 1833–1839.

19 Z. P. Jovanov, H. A. Hansen, A. S. Varela, P. Malacrida, A. A. Peterson, J. K. Nørskov, I. E. Stephens and I. Chorkendorff, *Journal of Catalysis*, 2016, **343**, 215–231.

20 M. Zhong, K. Tran, Y. Min, C. Wang, Z. Wang, C.-T. Dinh, P. De Luna, Z. Yu, A. S. Rasouli, P. Brodersen, S. Sun, O. Voznyy, C.-S. Tan, M. Askerka, F. Che, M. Liu, A. Seifitokaldani, Y. Pang, S.-C. Lo, A. Ip, Z. Ulissi and E. H. Sargent, *Nature*, 2020, **581**, 178–183.

21 A. A. Peterson and J. K. Nørskov, *Journal of Physical Chemistry Letters*, 2012, **3**, 251–258.

22 H. Xiang, S. Rasul, K. Scott, J. Portoles, P. Cumpson and E. H. Yu, *Journal of CO2 Utilization*, 2019, **30**, 214–221.

23 Metrohm, *Nova*, https://www.metrohm.com/en_gb/service/software-center/nova.html.

24 B. C. Marepally, C. Ampelli, C. Genovese, F. Tavella, E. A. Quadrelli, S. Perathoner and G. Centi, *Journal of CO2 Utilization*, 2020, **35**, 194–204.

25 J. Choi, M. J. Kim, S. H. Ahn, I. Choi, J. H. Jang, Y. S. Ham, J. J. Kim and S.-K. Kim, *Chemical Engineering Journal*, 2016, **299**, 37–44.

26 M. B. Kale, R. A. Borse, A. Gomaa Abdelkader Mohamed and Y. Wang, *Advanced Functional Materials*, 2021, **31**, 2101313.

27 R. Reske, H. Mistry, F. Behafarid, B. Roldan Cuenya and P. Strasser, *Journal of the American Chemical Society*, 2014, **136**, 6978–6986.

28 M. Claros, M. Setka, Y. P. Jimenez and S. Vallejos, *Nanomaterials*, 2020, **10**, 471.

29 E. Cano, M. F. López, J. Simancas and J. Bastidas, *Journal of The Electrochemical Society*, 2001, **148**, E26.

30 V. Nikesh, A. Mandale, K. Patil and S. Mahamuni, *Materials research bulletin*, 2005, **40**, 694–700.

31 C. Mosser, A. Mosser, M. Romeo, S. Petit and A. Decarreau, *Clays and Clay Minerals*, 1992, **40**, 593–599.

32 S. Contarini and L. Kevan, *The Journal of Physical Chemistry*, 1986, **90**, 1630–1632.

33 D. Cahen, P. Ireland, L. Kazmerski and F. Thiel, *Journal of applied physics*, 1985, **57**, 4761–4771.

34 J. Liu, S. Li, B. Zhang, Y. Wang, Y. Gao, X. Liang, Y. Wang and G. Lu, *Journal of colloid and interface science*, 2017, **504**, 206–213.

35 M. Faur, M. Faur, D. Jayne, M. Goradia and C. Goradia, *Surface and Interface Analysis*, 1990, **15**, 641–650.

36 Z. M. Detweiler, J. L. White, S. L. Bernasek and A. B. Bocarsly, *Langmuir*, 2014, **30**, 7593–7600.

37 Y.-R. Lin, Y.-C. Chang and F.-H. Ko, *International Journal of Hydrogen Energy*, 2023.

38 G. Marcandalli, M. C. Monteiro, A. Goyal and M. T. Koper, *Accounts of chemical research*, 2022, **55**, 1900–1911.

39 K. J. P. Schouten, E. Pérez Gallent and M. T. M. Koper, *Journal of Electroanalytical Chemistry*, 2014, **716**, 53–57.

40 S. Nitopi, E. Bertheussen, S. B. Scott, X. Liu, A. K. Engstfeld, S. Horch, B. Seger, I. E. L. Stephens, K. Chan, C. Hahn,

J. K. Nørskov, T. F. Jaramillo and I. Chorkendorff, *Chemical Reviews*, 2019, **119**, 7610–7672.

41 R. Reske, M. Duca, M. Oezaslan, K. J. P. Schouten, M. T. Koper and P. Strasser, *The Journal of Physical Chemistry Letters*, 2013, **4**, 2410–2413.

42 M. Gattrell, N. Gupta and A. Co, *A review of the aqueous electrochemical reduction of CO_2 to hydrocarbons at copper*, 2006.

43 E. Pérez-Gallent, G. Marcandalli, M. C. Figueiredo, F. Calle-Vallejo and M. T. Koper, *Journal of the American Chemical Society*, 2017, **139**, 16412–16419.

44 J. Xie, X. Yang and Y. Xie, *Nanoscale*, 2020, **12**, 4283–4294.

45 F. Calle-Vallejo and M. T. Koper, *Angewandte Chemie - International Edition*, 2013, **52**, 7282–7285.

46 J. H. Montoya, C. Shi, K. Chan and J. K. Nørskov, *Journal of Physical Chemistry Letters*, 2015, **6**, 2032–2037.

47 X. Nie, M. R. Esopi, M. J. Janik and A. Asthagiri, *Angewandte Chemie - International Edition*, 2013, **52**, 2459–2462.

48 D. W. DeWulf, T. Jin and A. J. Bard, *Journal of the Electrochemical Society*, 1989, **136**, 1686.

49 K. J. Schouten, Y. Kwon, C. J. Van Der Ham, Z. Qin and M. T. Koper, *Chemical Science*, 2011, **2**, 1902–1909.

50 D. Kim, C. S. Kley, Y. Li and P. Yang, *Proceedings of the National Academy of Sciences*, 2017, **114**, 10560–10565.